Phys. Scr. **76** (2007) C115–C121 doi:10.1088/0031-8949/76/3/N18

Steady-state and time-resolved two-photon fluorescence microscopy: a versatile tool for probing cellular environment and function

Stefan Denicke[1], Jan-Eric Ehlers[1], Raluca Niesner[1,2], Stefan Quentmeier[1] and Karl-Heinz Gericke[1]

[1] Institute of Physical and Theoretical Chemistry, Technical University of Braunschweig, Hans-Sommer Straße 10, D-38106 Braunschweig, Germany
[2] Helmholtz Centre for Infection Research, Inhoffenstraße 7, D-38124 Braunschweig, Germany

E-mail: k.gericke@tu-braunschweig.de

Received 12 February 2007
Accepted for publication 21 May 2007
Published 13 August 2007
Online at stacks.iop.org/PhysScr/76/C115

Abstract
In the last decade, the two-photon fluorescence laser-scanning microscopy (TPLSM) has become an indispensable tool for the bioscientific and biomedical research. TPLSM techniques as well as their applications are currently experiencing a dramatic evolution and represent the focus of many biophysical research projects. In this work, we compare in detail two steady-state TPLSM techniques, i.e. single-beam scanning microscopy combined with point-detection (SB-PMT) and multi-beam scanning microscopy combined with synchronous detection (MB-CCD), as far as their technical characteristics relevant for the bioscientific research are concerned, i.e. optical performance and imaging speed. We demonstrate that the SB-PMT technique is more adequate for deep-tissue imaging (few 100 μm depth) than the MB-CCD technique, whereas only the MB-CCD technique enables high-speed imaging for characterizing the dynamics of fast biological phenomena. Novel applications of these techniques are additionally discussed. Moreover, we employ a time-resolved TPLSM technique, i.e. biexponential fluorescence lifetime imaging based on the cellular fluorescence of the nicotinamide pyridine dinucleotides NADH and NADPH, which allows us to probe for the first time the redox cellular metabolism of MIN6 cells (mutated insulin producing pancreatic β-cells) as well as to show the potential of this method for the specific and dynamic investigation of NADH- and NADPH-dependent cellular processes.

PACS numbers: 87.64.Ni, 87.64.Vv, 87.64.Rr

(Some figures in this article are in colour only in the electronic version.)

M This article features online multimedia enhancements

1. Introduction

Since its development in the early 1990s, two-photon laser-scanning microscopy (TPLSM) has experienced a breakthrough in the non-invasive high-quality imaging of biological systems [1]. This technique is based on simultaneous two-photon excitation of molecules present inside the observation volume followed by the detection of their fluorescence. The applications of steady-state TPLSM, i.e. TPLSM based on the measurement of the integral flurorescence signal, reach from 3D morphology investigations in intact tissue and organs [2, 3] to dynamical studies of cell–cell interactions [4–6] as well as of tissue and organ function [7] in important bioscientific branches, e.g. neurosciences, dermatology, immunology, and

diabetes research. Furthermore, TPLSM represents the basis of many other fluorescence techniques, e.g. ratiometric microfluorimetry, fluorescence lifetime imaging (FLIM) and fluorescence anisotropy imaging, with great applicative potential for the biosciences.

The advantages of TPLSM over standard one-photon excitation fluorescence microscopic techniques, e.g. confocal microscopy or wide-field microscopy, are the intrinsic 3D resolution, a large penetration depth in thick highly-scattering biological media and a low photobleaching and photodamage of the sample outside the focal plane [1, 8]. These advantages are to be derived from the principal characteristics of the two-photon excitation. The low two-photon excitation cross-section (typically, $10^{-50}\,\mathrm{cm}^4\,\mathrm{s}$ as compared to one-photon excitation cross-sections of $10^{-17}\,\mathrm{cm}^2$) and the quadratic dependence of the excitation rate on the illumination photon flux lead to a 3D-confined excitation volume and, thus, to almost no photoprocesses in the out-of-focus regions. Since biological tissue can be more easily penetrated by near infrared (NIR) than by visible or ultraviolet light, the necessity of using NIR illumination for the two-photon excitation lead to a large penetration depth in this kind of sample [9, 10]. However, low two-photon excitation cross-sections also lead to the main drawback of TPLSM, i.e. the need of high photon fluxes for adequate excitation rates. This drawback is counteracted by the use of ultra-short (femtosecond) pulsed lasers, characterized by a low averaged energy in spite of high photon fluxes during the laser pulse [1].

Currently, steady-state TPLSM techniques based on scanning of the sample with a single laser beam followed by fluorescence detection by means of photomultiplier tubes (PMTs), i.e. point detection, are largely employed in biosciences [11]. However, due to the fact that these methods are too slow to track the dynamics of important biological processes, alternative techniques based on a faster multi-beam scanning combined with synchronous fluorescence detection, e.g. that of CCD cameras, have been developed [12]. In this work we compare in detail a standard single-beam PMT with a multi-beam CCD technique, as far as the technical characteristics important for the bioscientific research are concerned, i.e. optical performance and imaging speed. Moreover, we present novel applications of these TPLSM methods of particular relevance for the immunology.

While 3D-morphology and cell–cell interaction studies can be accurately performed using steady-state procedures, the investigation of the cellular function on subcellular basis is possible only by means of time-resolved TPLSM procedures, e.g. FLIM. FLIM allows the investigation of cellular parameters [13–15], e.g. refractive index, pH, ions and oxygen concentration, viscosity, as well as the elucidation of vital processes like redox metabolism, photosynthesis in green plants or fluorescence resonant energy transfer between endogenous macromolecules [16–18].

The principal methods of measuring the fluorescence decay time in an image are frequency-domain techniques [19, 20] and time-domain techniques, e.g. time correlated single-photon counting (TCSPC) [21] or time-gating procedures [22]. Among these, time-domain FLIM techniques, i.e. direct methods, are more favourable due to their accuracy and rapidity in data-acquisition and evaluation. Time-gating procedures are particularly adequate for dynamic investigations of fast biological processes since they are based on synchronous signal detection (CCD detection), however, they have the disadvantage of using only 10–15% of the total fluorescence signal. In contrast, TCSPC methods use the signal much better (up to 100%) and, thus, enable the investigation of poorly fluorescing samples. However, since they are based on PMT point-detection, they are much slower than the time-gating techniques.

In this work, we use a time-gating technique to probe for the first time the redox cellular metabolism of mutated insulin-producing pancreatic β-cells (MIN6 cells) by means of biexponential FLIM based on the endogenous fluorescence of the coenzymes nicotinamide adenine dinucleotide (NADH) and nicotinamide adenine dinucleotide phosphate (NADPH), hereafter NAD(P)H. This method satisfies particularly well the typical bioscientific requirements, i.e. a high gain on information about the system under study without disturbing its natural environment. The reasons therefore are twofold: the considered method is label-free and it allows a direct and detailed insight in important cellular phenomena. Moreover, we made observations, which indicate that a specific and dynamic visualization of NAD(P)H-dependent cellular processes is possible by using the selectivity of the catalysator-enzymes, to which NAD(P)H is bound.

2. Experiment

All experiments were carried out using a specialized TPLSM based on a tunable (720–920 nm) Ti : Sa laser (MaiTai, Spectra Physics, Darmstadt, Germany) and on a commercial scan-head (TriMScope, LaVision BioTec, Bielefeld, Germany), which allows both single-beam as well as multi-beam (2, 4, ... or 64 beamlets) scanning of the sample. The multi-beam scanning permits a speed-up of data acquisition proportional to the splitting of the main laser beam. The excitation beam is focused into the sample by a $20\times$ objective lens with $\mathrm{NA} = 0.95$ and a working distance of 2 mm (Olympus, Hamburg, Germany). In steady-state experiments we employed as a detection unit either a PMT (LaVision Biotec) for single-beam scanning or a CCD camera (Sensicam QE, LaVision, Göttingen, Germany) for multi-beam scanning. In FLIM experiments the fluorescence signal was detected using an intensified CCD camera with variable time-gate (200–1000 ps) (PicoStar, LaVision).

Intravital experiments (blood flow visualization in living mice) as well as experiments on neutrophil granulocytes from the bone marrow of balb/c mice, on mouse spleen and on enhanced yellow fluorescing protein (EYFP) expressing brain slices from mouse were performed in collaboration with M Gunzer from the Helmholtz Centre for Infection Research, Braunschweig. The MIN6 were provided by I Rustenbeck (Institute of Pharmacology and Toxicology, Technical University Braunschweig).

Cell staining was performed with 5 μM saline solutions either of CFSE (carboxyfluoresceine succinimide-ester) or of cell tracker orange (CTO) (Invitrogen, Karlsruhe, Germany). For intravital experiments, rhodamine 6G was intravenous (iv) injected in the mouse.

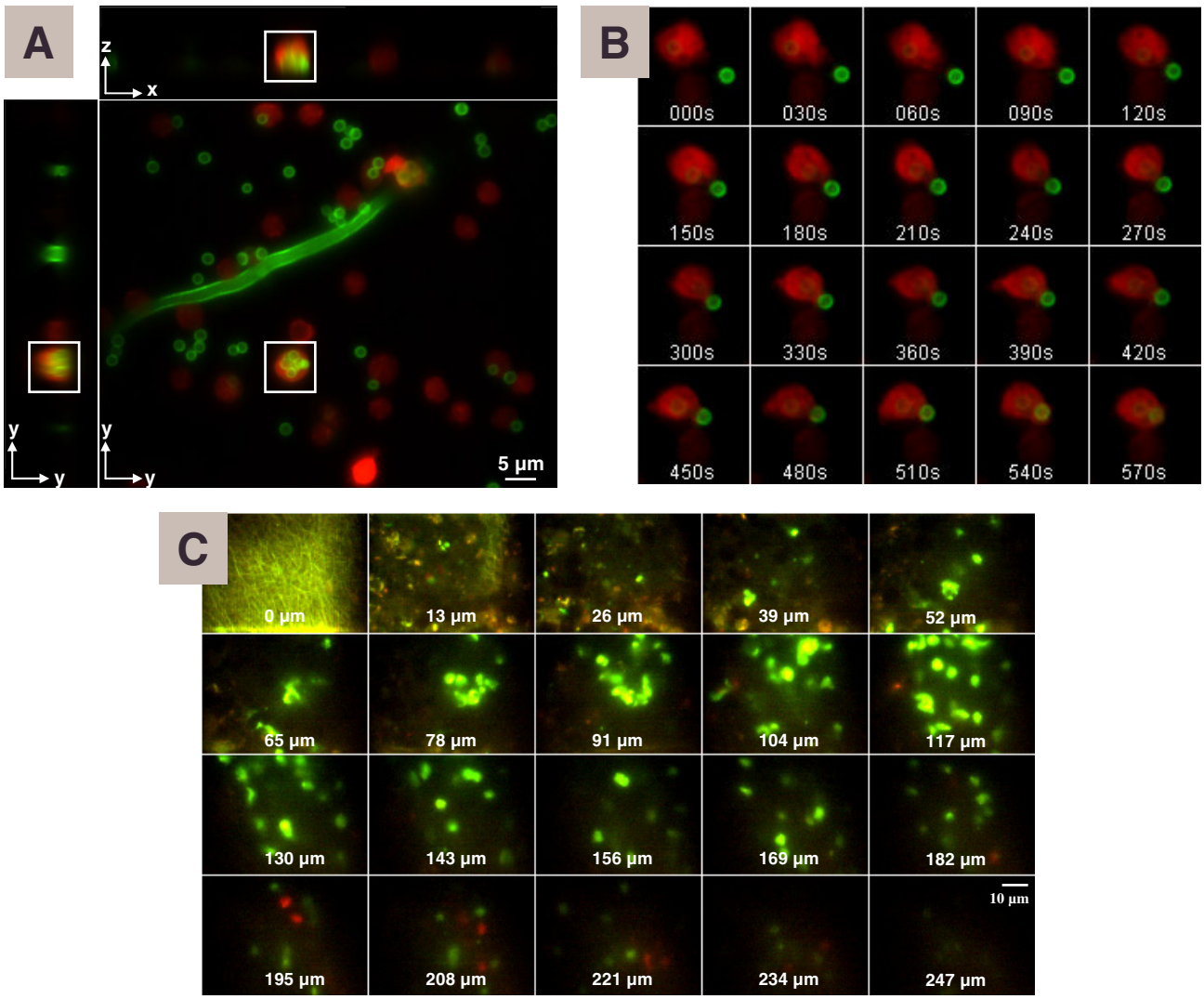

Figure 1. (A) *xy*-, *xz*- and *yz*-perspectives of a 3D image representing neutrophil granulocytes phagocyting conidia (round) and a hypha (ribbon-shaped), i.e. spores and the adult form of the fungus *A. fumigatus*, respectively. The different perspectives of the framed neutrophil granulocyte univocally indicate that conidia were internalized by the cell, i.e. they were phagocyted. The fluorescence of the CTO stained neutrophil granulocytes (red) was observed at 590 ± 25 nm, while that of the CFSE stained fungus (green) was observed at 535 ± 25 nm. (B) Time series of 2D fluorescence images (similar to A) representing the actual process of phagocytosis over approximately 10 min. (C) Two-colour fluorescence images in an intact spleen of a mouse, in which CTO stained B-cells (red) and CFSE stained T-cells (green) were previously injected. Note that T-cells predominate at the surface (down to 180 μm depth), while in deeper layers B-cells appear more frequently. The collagen and elastin cuticula of the spleen (yellow) appears in both emission channels. The z-step between two consecutive images is 13 μm.($\lambda_{exc} = 800$ nm). (Movie 1. 3D-movie representing CTO stained neutrophil granulocytes (red) phagocyting the CFSE stained fungus *Aspergillus fumigatus* (green). ($\lambda_{exc} = 800$ nm). Available at stacks.iop.org/PhysScr/76/C115.)

Point-spread function (PSF) experiments were performed using blue (440 nm) and yellow-green (515 nm) fluorescing polystyrene beads of 100 nm in diameter, respectively (Invitrogen).

3. Results and discussion

3.1. Steady-state two-photon fluorescence microscopy

Due to its advantages over the standard confocal and wide-field microscopy, steady-state TPLSM has became over the last decade one of the most versatile tools for studies in complex biological systems, e.g. studies of cell–cell interactions in intact tissue or even in living organisms.

In order to underline the advantages of the TPLSM-procedures employed here and to give an insight into the potential of TPLSM, in general, we refer to two concrete applications of particular relevance for the immunology: the dynamical 3D-visualization of neutrophil granulocytes (cells of the unspecific immune system) phagocyting the fungus *Aspergillus fumigatus* and the 3D-imaging of mouse spleen containing T- and B-cells (the cells which are responsible for the acquired immunity).

3D TPLSM-experiments performed over time on mixed suspensions of neutrophil granulocytes and *A. fumigatus* (fungus spores (conidia) and adult form (hyphae)) allow univocal answers to central questions about the process of phagocytosis. They demonstrate that conidia are really internalized by the neutrophil granulocytes (figure 1(A)), show the interactions of neutrophil granulocytes with hyphae (movie 1), and elucidate the dynamics of phagocytosis (figure 1(B) and movie 1). A high spatial resolution (330 nm

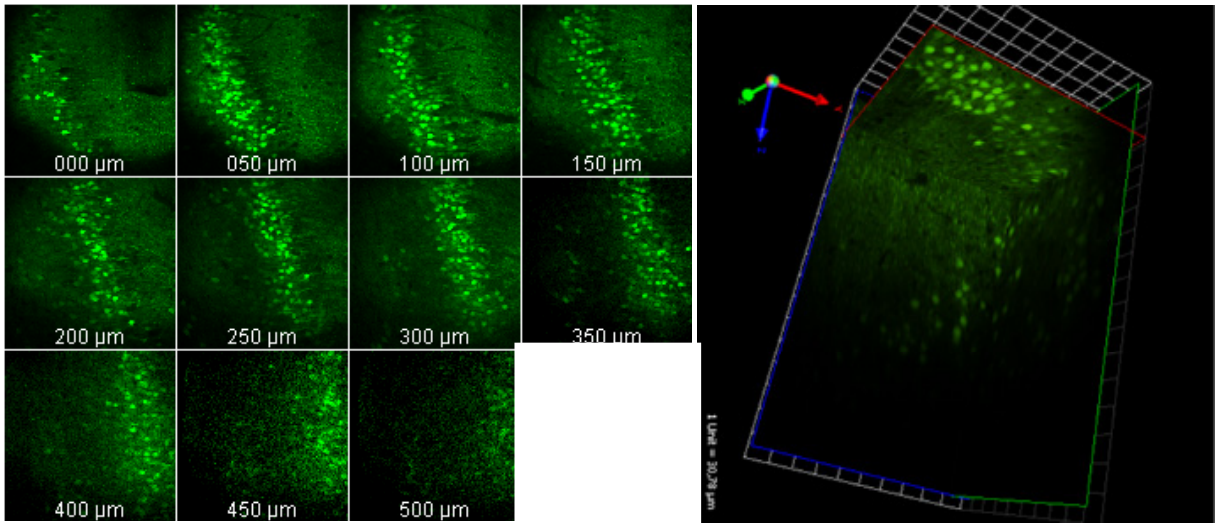

Figure 2. Fluorescence images ($300 \times 300\,\mu m^2$) in different depth layers (see inset) of an EYFP expressing brain slice (emission detected at 535 ± 25 nm). The somata of neurons are round-shaped, while the dendrites and the axons apear fiber-like. Note that the fluorescence signal as well as the SNR decreases with increasing penetration depth. ($o\lambda_{exc} = 920$ nm).

lateral and 1.4 μm axial) as well as a fast acquisition of 3D-datastacks (in this case, 30 s between two consecutive 3D-representations) is the reason for the success of these experiments.

Deep-tissue 3D-measurements in the spleen of mice, in which CTO-stained B-cells and CFSE-stained T-cells were previously injected, reveal the distribution of these cells in the organ under study (figure 1(C)). T-cells dwell at the surface of the spleen, whereas B-cells first appear in more than 120 μm depth. These TPLSM-measurements will enable the study of interaction mechanisms between B- and T-cells in their genuine environment and, thus, will contribute to the elucidation of the defence mechanisms in organism. The characteriztic of TPLSM, which first allow investigations in intact organs, is the large penetration depth (in this case $\sim$250 μm) due to NIR excitation ($\lambda_{exc} = 800$ nm).

All measurements were performed using the multi-beam (64 beamlets) CCD set-up at an excitation power of at most 10 mW per beamlet, which ensures negligible photodamage of the sample.

The experiments discussed above reveal the main requirements of the biosciences on high-end imaging technologies like the TPLSM. These are:

1. imaging in thick highly-scattering tissue as deep as possible without injuring the sample and
2. dynamically registering vital biological phenomena in their natural environment.

The two-photon microscopy, like all other imaging technologies, does not provide a unique solution for all bioscientific problems. However, two TPLSM-procedures, i.e. single-beam scanning combined with the point-detection of PMT and multi-beam scanning combined with the synchronous detection of CCD cameras, are of great interest when considering the requirements mentioned above. The potential of these procedures is investigated here, as far as their applicability for biological studies is concerned.

We first compare the spatial (lateral and axial) resolution of the two TPLSM-set-ups, which is given by the dimensions of the PSF of a point-object, i.e. with dimensions below the resolution limit. In our case, the point-objects were fluorescent polystyrene beads of 100 nm in diameter.

Measurements in agarose with a $20 \times$ lens (NA = 0.95) at $\lambda_{exc} = 800$ nm show that, as far as the spatial resolution is concerned, both set-ups are identical. The lateral resolution is 337 ± 23 nm for the multi-beam CCD set-up and 341 ± 24 nm for the single-beam PMT set-up, while the axial resolution is 1.37 ± 0.11 and 1.40 ± 0.19 μm, respectively. Neither the emission wavelength of the beads (440 and 515 nm, respectively) nor the penetration depth influence the resolution. Furthermore, PSF measurements in biologically relevant samples, i.e. brain tissue and lymph nodes, confirmed the similarity of the two TPLSM-procedures. However, in these samples we observed a dramatic degradation of the PSF with increasing penetration depth [23].

3.1.1. Deep-tissue imaging. The quality of deep-tissue imaging depends on two optical parameters related to each other, i.e. the maximum penetration depth and the signal-to-noise ratio (SNR). Due to scattering, the fluorescence signal decreases with increasing penetration depth, while the noise remains constant (figure 2). Consequently, the SNR follows the same decreasing trend. The maximum penetration depth is defined as the depth, in which the fluorescence signal reaches the noise level, i.e. SNR is equal to 1.

In EYFP expressing brain slices, a maximum penetration depth of 310 μm was attained by using the MB-CCD set-up, whereas 510 μm in depth could be imaged with the single-beam PMT set-up (figure 2).

These results indicate that deep-tissue imaging is possible by means of the two investigated TPLSM-procedures. However, the single-beam PMT set-up, characterized by a better SNR, is more adequate for imaging experiments in more than a few hundred microns depth.

3.1.2. High-speed imaging. Data acquisition at high optical quality is just one aspect of interest for studies in complex biological systems. Additionally, the acquisition should be

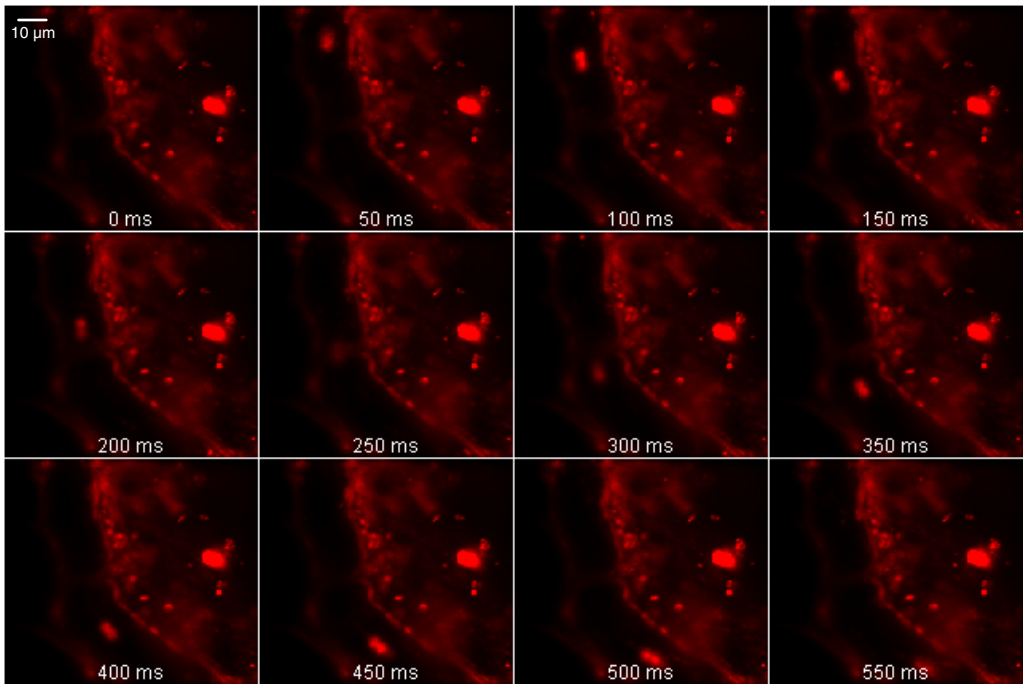

Figure 3. Time series of fluorescence images representing the blood flow in a mouse, in which rhodamine 6G was previously iv injected. Note the pair of rolling cells within the blood vessel, which are most likely lymphocytes. The imaging speed was 20 Hz. ($\lambda_{exc} = 800$ nm). (Movie 2. 2D movie of blood flow in a mouse, in which rhodamine 6G was previously iv injected. The small cells are erythrocytes or thrombocytes, while the larger (rolling) cells are lymphocytes. The imaging speed is 20 Hz. ($\lambda_{exc} = 800$ nm). Available at stacks.iop.org/PhysScr/76/C115.)

fast enough, so that process dynamics can be timely resolved. By using the single-beam PMT set-up, a fluorescence image of $150 \times 150\,\mu m^2$ ($20\times$ objective) is achieved after 5000 ms exposure time, while by using the multi-beam CCD set-up the same image can be achieved after only 83 ms. Thus, only the CCD set-up enables the investigation of ultra-fast phenomena frequently met in biosciences.

In order to demonstrate the speed of the multi-beam CCD system, we dynamically (2D and 3D) imaged the fluorescence of a blood vessel in living mice, in which rhodamine 6G (100 μl, 1.25 mM in 0.9% NaCl) was iv injected. The dye stained both the cells inside the vessel (e.g. erythrocytes, thrombocytes, lymphocytes), as well as the walls of the vessel and the surrounding tissue (figure 3). Thus, our experiments allow the visualization of high-speed cell–cell as well as cell-vessel interactions of particular interest for the immunology (figure 3 and movie 2). The imaging speed for a $50 \times 50\,\mu m^2$ region was 20 Hz, limited by the read-out of the CCD camera (50 ms).

Concluding, for *deep-tissue imaging* in whole organs or even in the intact organism, single-beam PMT microscopy is the most adequate method. While *high-speed imaging* of fast phenomena can only be achieved by using the multi-beam CCD system.

3.2. FLIM

As demonstrated both here and by other authors, the steady-state two-photon microscopy is a versatile tool in the investigation of tissue morphology as well as of cell–cell interactions in complex biological systems. However, studies of the cellular function mirrored in modifications of cellular parameters or in vital cellular processes, e.g. cellular metabolism, can only be quantitatively performed by using the advantages of time-resolved fluorescence microscopy. We refer here to FLIM in time-domain based on time-gating. This method relies on the acquisition of a series of time-gated intensity images at different time-points after the excitation laser pulse, so that in each pixel of the image, a fluorescence decay curve $F(t)$ is attained. The approximation of this decay curve by a sum of exponential functions (equation 1) best describes the photophysics inside the sample, i.e. each monoexponential decay curve corresponds to a fluorescent component.

$$F(t) = \sum_{i=1}^{n} a_i \cdot e^{-t/\tau_i}, \qquad (1)$$

τ_i is the fluorescence lifetime of the ith fluorescent component and a_i represents its contribution to the total fluorescence signal. n is the total number of fluorescent components in the sample. We excluded here the background, which is subtracted from $F(t)$ before performing the evaluation.

The temporal accuracy of our method was verified in FLIM-measurements on 4-[4-(dimethylamino)styryl]-1-methylpyridinium iodide (DASPI) solutions of different viscosities (mixtures of glycol and water). Modifications of the fluorescence lifetime of DASPI as small as 10 ps were measured.

3.2.1. Cellular redox metabolism. In order to probe the cellular metabolism by means of FLIM, we used as signal mediators the fluorescing coenzymes NADH and NADPH. These coenzymes are ubiquitous cellular electron carriers for enzyme-catalysed redox processes in the adenosine triphosphate (ATP) production as well as in reductive biosyntheses of macromolecules. In order to perform accurate

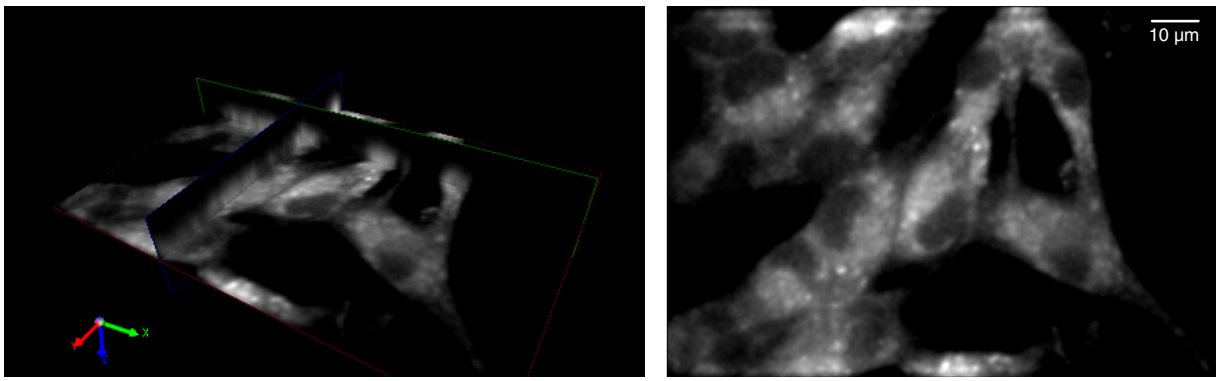

Figure 4. 2D and 3D NAD(P)H autofluorescence images of MIN6 cells. Note that the NAD(P)H fluorescence signal is low within the nuclei but large in small structures in the cytoplasma, i.e. mitochondria (emission at 460 ± 20 nm, $\lambda_{exc} = 760$ nm).

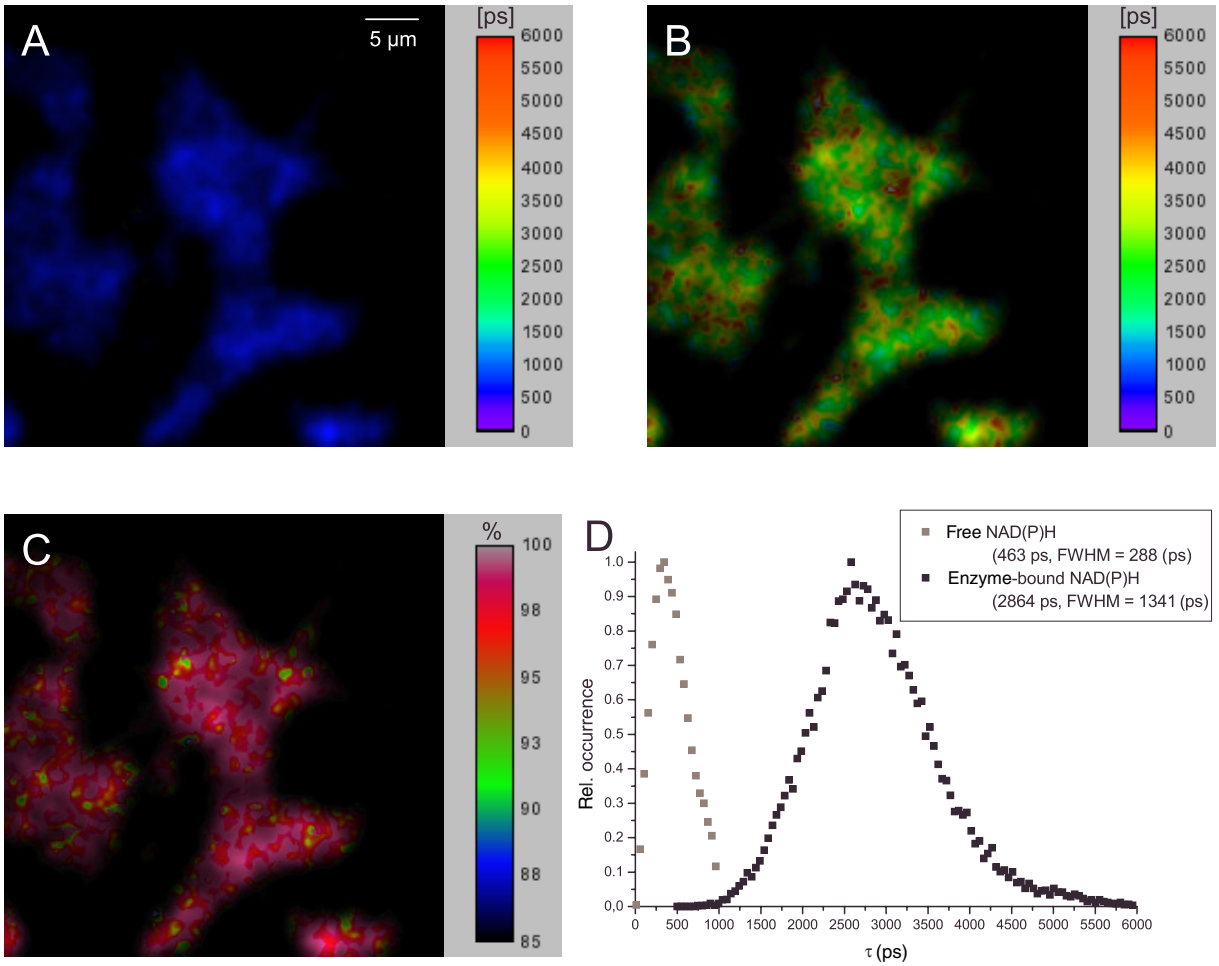

Figure 5. Biexponential FLIM based on NAD(P)H fluorescence in MIN6 cells. (A) fluorescence lifetime image of free NAD(P)H; (B) fluorescence lifetime image of enzyme-bound NAD(P)H; (C) ratio-image representing the contribution of the bound NAD(P)H to the total fluorescence signal, i.e. qualitative image of the redox cellular metabolism; (D) occurrence frequency of the fluorescence lifetimes in the images A and B.

FLIM experiments, we isolated the signal of NAD(P)H from that of other endogenous chromophores, e.g. melanin, serotonin, metaloporphyrins, by exciting the samples at 760 nm and observing the emission at 460 ± 20 nm. Under these conditions, more than 98% of the fluorescence within the cells originates from NAD(P)H. The fact that the cellular autofluorescence is low within the nuclei but high in small organelles (mitochondria) in cytosol (see figure 4) confirms this assumption.

NAD(P)H exists in two different states within the cell: either free, i.e. it does not participate in any cellular process, or enzyme-bound, i.e. it participates in vital redox processes catalysed by the enzymes, to which it is bound. Both states of NAD(P)H (free and enzyme-bound) fluorescence and are characterized by specific fluorescence lifetimes. Consequently, the NAD(P)H fluorescence decay curve is at least biexponential. Thus, by using biexponential FLIM we are able to extract from the NAD(P)H signal of MIN6

cells two major fluorescence lifetimes in each pixel of the image: that of free NAD(P)H at approximately 450 ps and that of enzyme-bound NAD(P)H at approximately 3000 ps (figures 5(A) and (B)).

In order to rapidly perform the biexponential FLIM evaluation (equation (2)), which first enables dynamical tracking of changes in the cellular function, we used a self-made non-iterative fitting method [16].

$$F(t) = a_{\text{free}} \cdot e^{-t/\tau_{\text{free}}} + a_{\text{bound}} \cdot e^{-t/\tau_{\text{bound}}}. \qquad (2)$$

Except for the FLIMs of the free resp. enzyme-bound NAD(P)H, a further result of the biexponential FLIM evaluation of the cellular NAD(P)H fluorescence is the ratio-image (figure 5(C)). It represents the contribution of the enzyme-bound NAD(P)H to the total fluorescence signal, i.e. $a_{\text{bound}}\tau_{\text{bound}}/(a_{\text{free}}\tau_{\text{free}} + a_{\text{bound}}\tau_{\text{bound}})$. Since the fluorescence signal of the free resp. bound NAD(P)H is proportional to their concentration, the ratio-image mirrors the redox activity of the cell and, thus, the cellular redox metabolism.

Note that while the fluorescence lifetime distribution of free NAD(P)H within the cell well reproduces the response function of the detection device, the distribution of the enzyme-bound NAD(P)H is considerably wider (figure 5(D)). Moreover, within a cell there are regions with different fluorescence lifetimes for bound NAD(P)H. All these observations indicate that, based on the fluorescence lifetime of the NAD(P)H-enzyme-complex, it is possible to specifically detect enzymes within the cell during their catalytic function only based on the fluorescence lifetime of the corresponding NAD(P)H-enzyme-complexes, as previously predicted by extracellular measurements [24, 25]. Since the coenzymes NADH and NADPH cannot indicate a specific cellular process, while the partner-enzymes enable such selectivity, the specific enzyme-detection directly lead to the ability of specifically and dynamically visualizing vital processes with submicron resolution and without disturbing the sensitive cellular balance. In future experiments, we plan to largely employ this method, e.g. for a better understanding of the mechanisms of insulin secretion in pancreatic β-cells as well as in the investigation of pathogen degradation in neutrophil granulocytes after phagocytosis.

4. Summary

By performing novel, biologically relevant investigations, i.e. studies on phagocytosis, on cellular metabolism of MIN6 cells and on cell–cell interactions in blood vessels as well as in spleen, we endorse in this work the potential of three techniques based on TPLSM, i.e. single-beam PMT microscopy, multi-beam CCD microscopy and time-gated FLIM. While the steady-state TPLSM-procedures are particularly adequate for morphology and cell–cell interactions studies, the time-resolved method (FLIM) allows probing of the cellular function.

As far as the applicability of steady-state TPLSM-procedures for bioscientifical research is concerned, we have demonstrated that single-beam microscopy based on PMT point-detection is the best solution for deep-tissue imaging in intact organs, whereas multi-beam microscopy based on CCD synchronous detection is the only solution for imaging fast biological phenomena.

We also show that biexponential FLIM based on endogenous NAD(P)H fluorescence is a versatile tool for probing cellular metabolism in MIN6 cells without the need for marker molecules. Moreover, this method offers the possibility to selectively and dynamically investigate NAD(P)H-dependent vital processes within the cell based on the specific fluorescence lifetime of NAD(P)H-enzyme-complexes.

Acknowledgments

We acknowledge the Bundesministerium für Bildung und Forschung for financial support under grant 0313412C (Bio-profile Hannover/Braunschweig/Göttingen) and our partners from the Joint Optical Metrology Centre, Braunschweig for fruitful discussions.

References

[1] Denk W, Strikler J H and Webb W W 1990 *Science* **248** 73–6
[2] Helmchen F and Denk W 2005 *Nat. Methods* **2** 232–40
[3] Corcuff P and Lévêque J-L 1993 *Dermatology* **186** 50–4
[4] Kerschensteiner M, Schwab M E, Lichtman J W and Misgeld T 2005 *Nat. Med.* **11** 572–7
[5] Kasthuri N and Lichtman J W 2004 *Curr. Opin. Neurobiol.* **14** 105–11
[6] Neumann J, Gunzer M, Gutzeit H, Ullrich O, Reymann K and Dinkel K 2006 *FASEB J.* **20** 714–6
[7] Germain R N, Miller M J, Dustin M L and Nussenzweig M C 2006 *Nat. Rev. Immunol.* **6** 497–507
[8] Gratton E, Barry N P, Beretta S and Celli A 2001 *Methods* **0** 103–10
[9] Koenig K 2000 *J. Microsc.* **200** 83–104
[10] So P T C, Kim H and Kochevar I E 1998 *Opt. Exp.* **3** 339–50
[11] Germain R N, Miller M J, Dustin M L and Nussenzweig M C 2006 *Nat. Rev. Immunol.* **6** 497–507
[12] Nielsen T, Fricke M, Hellweg D and Andresen P 2001 *J. Microsc.* **201** 368–76
[13] Lakowicz J R, Szmacinski H and Johnson M L 1992 *J. Fluorescence* **2** 47–62
[14] Niesner R, Peker B, Schlüsche P, Gericke K-H, Hofmann C, Hahne D and Müller-Goymann C 2005 *Pharm. Res.* **22** 1078–87
[15] Hanson K, Behne M, Barry N, Mauro T, Gratton E and Clegg R 2002 *Biophys. J.* **83** 1682–90
[16] Niesner R, Peker B, Schluesche P and Gericke K-H 2004 *Chem. Phys. Chem.* **5** 1141–9
[17] Barzda V, Grauw C, Vroom J, Kleima F, van Grondelle R, van Amerongen H and Gerritsen H 2001 *Biophys. J.* **81** 538–46
[18] Murata S, Herman P and Lakowicz J R 2001 *Cytometry* **43** 94–100
[19] Squire A, Verveer P J and Bastiaens P 2000 *J. Microsc.* **197** 136–49
[20] Gratton E, Breusegem S, Sutin J, Ruan Q and Barry N 2003 *J. Biomed. Opt.* **8** 381–90
[21] Becker W, Bergmann A, Biskup C, Kloecker N and Benndorf K 2002 *Proc. SPIE* **4620** 555
[22] Benny Lee K C, Siegel J, Webb S, Lévêque-Fort S, Cole M, Jones R, Dowling K, Lever M and French P 2001 *Biophys. J.* **81** 1265–74
[23] Niesner R, Andresen V, Neumann J, Spiecker H and Gunzer M 2007 *Biophys. J.* at press
[24] Gafni A and Brand L 1976 *Biochemistry* **15** 3165–71
[25] Jameson D M, Thomas V and Zhou D 1989 *Biochim. Biophys. Acta* **994** 187–90